

Absorption and analysis of unbound quantum particles – one by one

Sølve Selstø¹

¹*Faculty of Technology, Art and Design, Oslo Metropolitan University, NO-0130 Oslo, Norway*

In quantum physics, the theoretical study of unbound many-body systems is typically quite complex – owing to the combination of their large spatial extension and the so-called *curse of dimensionality*. Often, such systems are studied on truncated numerical domains – at the cost of losing information. Here we present methods for calculating differential probabilities for unbound particles which are subjected to a *complex absorbing potential*. In addition to attenuating outgoing waves, this absorber is also used to probe them by projection onto single-particle scattering states, thus rendering the calculation of multi-particle scattering states superfluous. Within formalism based on the Lindblad equation, singly differential spectra from subsequent absorptions are obtained by resolving the dynamics of the remaining particles after the first absorption. While the framework generalizes naturally to any number of particles, explicit, compact and intuitive expressions for the differential probability distributions are derived for the two-particle case. The applicability of the method is illustrated by numerical examples involving two-particle model-systems. These examples, which address scattering and photo ionization, demonstrate how energy distributions of unbound particles may be determined on numerical domains considerably smaller than the actual extension of the system.

I. INTRODUCTION

Simulating quantum many-body dynamics is often a hard endeavour. One reason for this is the fact that the complexity of such studies grows exponentially with the number of particles; this is the infamous *curse of dimensionality*. For unbound many-body quantum systems it becomes even worse as the extension of the systems under study is not limited. The numerical study of such systems requires a very high number of degrees of freedom – for each particle. Combined with the curse of dimensionality, this renders several interesting simulations unfeasible.

A much applied way of dealing with the unbounded nature of the wave function is to impose absorbing boundary conditions. Such boundary conditions allow us to remove outgoing waves, corresponding to unbound particles, and truncate the numerical domain without introducing artifacts such as, e.g., reflections at the boundary or wave packets reappearing at the opposite edge of the grid, as would be the case with periodic boundary conditions. Absorbing boundaries may be introduced in several ways [1]; *exterior complex scaling* [2] or the closely related notion of *perfectly matched layers* [3] are frequently used techniques. Another one is to introduce a masking function in the propagation scheme [4–7], or, equivalently, to augment the Hamiltonian with a complex absorbing potential, a *CAP*, which vanishes in some interior region [8–17]. Such a potential could, like exterior complex scaling, depend on both position and momentum, or it could be a purely position-dependent potential. In this work, we will exclusively deal with the latter.

When a simulation of a dynamical quantum systems is subjected to absorption, information is lost during the course. In a many-body setting, this loss is devastating for simulations based on the Schrödinger equation alone; if one particle is absorbed, the entire wave function is lost. No information remains about the remaining sub-system. While this issue is resolved by the Lindblad equation [18, 19], the resulting equation of motion is still such that the information about the absorbed particles is discarded. However, since we know pre-

cisely what is removed from one instant to the next, it should be possible to analyse this removed part as it is absorbed. By aggregating such contributions from each time step, information such as, e.g., the energy spectrum of the unbound particles should be obtainable even on a truncated numerical grid. This is what we aim to do in this paper.

This is, of course, by no means any new endeavor. Several interesting methods for obtaining energy or angle resolved information about unbound particles using truncated numerical grids are put forward, see, e.g., [5, 20–33]. These methods have enabled several interesting physical studies within atomic, molecular and optical physics, see, e.g., [34–50] – only to name a few.

Some of these methods are, however, restricted to specific frameworks, such as formulations based on Hartree-Fock orbitals with a truncated number of excitations. Others approaches seem to ensure conservation of probability by somewhat pragmatic means. It is also fair to say that some of them tend to be rather complex and technical, thus resulting in a scheme which is demanding in terms of comprehension and/or implementation, and others do not seem to have any clear generalization beyond the one-particle context. For many-particle systems, on the other hand, methods tend to rely on projection onto scattering states with the same number of particles as the original system – approximative or exact ones. Obtaining these scattering states is usually quite involved, although some of the methods allows for projection onto uncorrelated product states.

For the above reasons, we believe that the present approach do have something to add to this rich flora of methods. It involves projections onto single-particle scattering states only – irrespective of the initial number of particles involved. This introduces a significant reduction in complexity since it evades the need for calculating many-particle scattering states, which in general involve several, possibly multiple or even time-dependent, continua. The ability to analyse the unbound particles using single-particle scattering states relies on the fact that the absorber is a one-particle operator. It only removes one particle at a time, and no two-particle interaction is involved in the absorption process. Thus, it is sufficient

to use single-particle scattering states in order to analyse what has been removed. In this sense, the singly differential spectra obtained uses the CAP actively to *probe* the outgoing waves. We will demonstrate how differential information about unbound particles can be obtained by accumulating information about the particles which are absorbed – one by one. Our approach provides a generic and intuitive scheme which generalizes naturally to any number of particles. Moreover, analyzing the outgoing waves introduces little extra effort in terms of implementation, computation and memory requirements. A drawback may be that it produces a sequence of singly differential probability distributions only. In order to describe remaining particles after the first absorption, a dynamical equation involving a density matrix rather than a wave function must be solved.

In the next section, the method is explained in detail. Explicit formulas are derived for the two-particle case. In Sec. III, we illustrate the scheme by applying it to two specific model systems, one involving scattering and another involving photo ionization. Conclusions are drawn in Sec. IV.

II. THEORY

Our starting point is a quantum system consisting of N identical particles. We impose absorbing boundaries by adding a CAP to the Hamiltonian. The resulting effective Hamiltonian is then

$$H_{\text{eff}} = H - i\Gamma, \quad (1)$$

where the actual Hamiltonian, H , and the CAP, Γ , are both Hermitian. Moreover, Γ is positive semi-definite. In a many-body context, it is convenient to express the interactions in terms of second quantization; this allows us to write up H and Γ in a manner which does not explicitly depend on the number of particles. We assume that H contains interactions between at most two-particles, while the CAP, Γ , is a one-particle operator. With a local potential the CAP is diagonal in position representation. Specifically,

$$\Gamma = \int \gamma(x) \hat{\psi}^\dagger(x) \hat{\psi}(x) dx, \quad (2)$$

where $\hat{\psi}(x)$ annihilates a particle with the position coordinates of x while $\hat{\psi}^\dagger(x)$ creates a particle with coordinates of x . For identical fermions these field operators obey the usual anti-commutation rule

$$\left\{ \hat{\psi}(x), \hat{\psi}^\dagger(x') \right\} = \delta(x - x'), \quad (3)$$

where the anti-commutator is replaced by a commutator in the case of identical bosons. Here “ x ” is taken to mean *all* degrees of freedom, including position, for each particle, and “ $\int \cdot dx$ ” refers to the definite integral or sum over the entire domain.

The CAP function $\gamma(x)$ is assumed to be zero within some finite interaction region and positive beyond. We will, as mentioned, take it to depend exclusively on the spatial coordinates.

It is usually imposed in order to avoid artifacts such as reflections at the boundary. In case of to strong a CAP, hard absorption may still induce reflections, however. As the CAP is not introduced on physical grounds, any dependence on Γ in the results of numerical simulations is unphysical. Results of simulations which prevail in the limit that Γ vanishes, may, however, be considered physical and correct.

A. Absorption from an N -particle system

The evolution of the system subjected to the CAP is governed by a non-Hermitian Schrödinger equation,

$$i\hbar \frac{d}{dt} |\Psi_N(t)\rangle = H_{\text{eff}} |\Psi_N(t)\rangle, \quad (4)$$

where the index N indicates the number of particles. In going from time t to $t + \tau$, the state evolves into

$$|\Psi_N(t + \tau)\rangle = |\Psi_N(t)\rangle - \frac{\tau}{\hbar} i H |\Psi_N(t)\rangle - \frac{\tau}{\hbar} \Gamma |\Psi_N(t)\rangle \quad (5)$$

to leading order in τ . The last term above leads to depletion of the original N -particle system; the part $-\tau/\hbar \Gamma |\Psi_N(t)\rangle$ has been removed in this time step. Since we know what we remove, we can also *analyse* this removed part. Specifically, one could project this part onto the appropriate scattering states and accumulate their contributions over time. Naively, this would correspond to accumulating contributions of the form

$$\left| \langle \varphi_\varepsilon^N | \frac{\tau}{\hbar} \Gamma | \Psi_N \rangle \right|^2, \quad (6)$$

where “ ε ” specifies the set of physical quantities of interest for the N -particle scattering state $|\varphi_\varepsilon^N\rangle$. This is indeed naive since such contributions, being of order τ^2 , would certainly not integrate to the total probability of absorption. Alternatively, one could integrate such contributions in time in a coherent manner. It is not obvious, however, how such a formulation would be consistent with norm conservation either.

Instead, it is more instructive to consider the density matrix $\rho_N = |\Psi_N\rangle \langle \Psi_N|$. The evolution of Eq. (4) may equivalently be described by the non-Hermitian von Neumann equation:

$$i\hbar \frac{d}{dt} \rho_N = H_{\text{eff}} \rho_N - \rho_N H_{\text{eff}}^\dagger = [H, \rho_N] - i\{\Gamma, \rho_N\}. \quad (7)$$

Now, in going from time t to $t + \tau$, the part which has been removed from the density matrix is, again, to leading order

$$\frac{\tau}{\hbar} \{\Gamma, \rho_N\}, \quad (8)$$

which contributes

$$\frac{\tau}{\hbar} \langle \varphi_\varepsilon^N | \{\Gamma, \rho_N\} | \varphi_\varepsilon^N \rangle = \frac{2\tau}{\hbar} \Re \langle \varphi_\varepsilon^N | \Gamma | \Psi_N \rangle \langle \Psi_N | \varphi_\varepsilon^N \rangle \quad (9)$$

to the ε -differential probability distribution of the absorbed particle. In this formulation, the resulting differential probability indeed provides the total absorption probability when

integrated over time and ε . In the limit that the CAP vanishes, its time integral should converge to the, possibly multiply, differential probabilities corresponding to the first absorption event.

In this work we will, however, take a different route. Firstly, we will reformulate the projections in terms of projection onto single-particle scattering states and, secondly, we will also calculate the differential probability distributions arising from subsequent absorption of multiple particles. As will be explained, the latter comes about via the Lindblad equation.

Instead of projection onto N -particle scattering states, as in Eq. (9), we integrate out all degrees of freedom for all but one of the identical particles and then analyze the remaining one. This may be done by means of field operators. The time derivative of the singly differential probability distribution, $\partial P/\partial \varepsilon$, can, accordingly, be expressed as

$$\hbar \frac{d}{dt} \frac{\partial P}{\partial \varepsilon} = \int \int \cdots \int_{N-1} \langle \varphi_\varepsilon | \hat{\psi}(x) \hat{\psi}(x') \cdots \hat{\psi}(x^{(N-1)}) \{ \Gamma, \rho_N \} (10) \\ \times \hat{\psi}^\dagger(x^{(N-1)}) \cdots \hat{\psi}^\dagger(x') \hat{\psi}^\dagger(x) | \varphi_\varepsilon \rangle dx dx' \cdots dx^{(N-1)},$$

where $|\varphi_\varepsilon\rangle$ now is a single-particle scattering state corresponding to the single physical quantity ε . The choice of naming it “ ε ” reflects the fact that *energy* is often the quantity in question; it could, however, be any relevant quantity.

We should also address another issue, from which both Eq. (9) and (10) suffer. The fact that both Γ and ρ_N are Hermitian, ensures that the anti-commutator $\{\Gamma, \rho_N\}$ is also Hermitian, and, thus, any diagonal element of this operator is real. However, although Γ and ρ_N are both positive semi-definite, the commutator $\{\Gamma, \rho_N\}$ is not necessarily so. Thus, diagonal elements such as $\langle \varphi_\varepsilon^N | \{\Gamma, \rho_N\} | \varphi_\varepsilon^N \rangle$ are not manifestly non-negative, which, in turn, makes their interpretation in terms of probabilities dubious. However, as mentioned, physical results are to be obtained in the limit that the CAP vanishes. As we will see in the numerical examples in Sec. III, the problem of “negative probabilities” vanishes in this limit.

B. Differential probability distributions from subsequent absorptions

When one out of N particles is absorbed in a simulation as dictated by the Schrödinger equation with a non-Hermitian effective Hamiltonian, Eq. (4), the wave function vanishes. It is certainly not converted into any $(N-1)$ -particle wave function. All information about the evolution of the remaining particles is lost. As mentioned, this problem is remedied by the Lindblad equation. Since absorption is in fact a Markovian process and trace and complete positivity should be conserved, the Lindblad equation is the proper starting point. The details on how to accommodate for particle removal by a CAP are provided in [51], while an adaption to the multi-configurational time-dependent Hartree-Fock-method is provided in [52].

The resulting equations of motion constitute a hierarchy of n -particle sub-systems, with $n = N, N-1, \dots, 1, 0$. The

evolution of the n -particle sub-system is governed by the master equation

$$i\hbar \frac{d}{dt} \rho_n = [H, \rho_n] - i\{\Gamma, \rho_n\} + 2i\mathcal{S}[\rho_{n+1}], \quad (11)$$

where the source term

$$\mathcal{S}[\rho] = \int \gamma(x) \hat{\psi}(x) \rho \hat{\psi}^\dagger(x) dx. \quad (12)$$

For an initial N -particle state, there is no source term and Eq. (11) reduces to Eq. (7), which, for a pure state, is equivalent to the Schrödinger equation, Eq. (4). As the first particle undergoes absorption at a certain probability, the source term, Eq. (12), populates the $(N-1)$ -particle sub-system in a manner which ensures that the total population of the N and the $(N-1)$ -particle remains unity in sum. As yet another particle is absorbed, also the $(N-2)$ -particle density matrix is populated – and so on. This way, one may, e.g., distinguish between single and double ionization probabilities of atoms without resorting to many-body scattering states nor numerical domains extending far into the asymptotic region [53].

As a particle is removed from the n -particle sub-system, ρ_n , by the absorber, it may be analyzed completely analogously to Eq. (10) by simply replacing N by n in the formula. In doing so we must, however, take some care in order to avoid double counting.

In the following, we will explain this in detail for the case of $N = 2$. We will also develop explicit formulas for the differential probability distributions corresponding to one and two absorptions from the original two-particle system.

C. The two-particle case

With an initial two-particle system, Eq. (10) may be written in a rather compact form. In App. A it is derived how Eq. (10) with $N = 2$ for an initial pure state leads to the following expression for the differential probability distribution:

$$\hbar \frac{d}{dt} \frac{dP}{d\varepsilon} = \int \langle \varphi_\varepsilon | \hat{\psi}(x) \{ \Gamma, \rho_2 \} \hat{\psi}^\dagger(x) | \varphi_\varepsilon \rangle dx = \\ 2 \int \int \varphi_\varepsilon(x)^* \varphi_\varepsilon(x') (\gamma(x) + \gamma(x')) \\ \times \int dy \Psi_2(x, y) \Psi_2^*(x', y) dy dx dx' \\ + 4 \int \gamma(x) \left| \int \varphi_\varepsilon^*(y) \Psi_2(x, y) dy \right|^2 dx. \quad (13)$$

Here $\Psi_2(x_1, x_2)$ is the two-particle wave function in product state representation, cf. Eq. (A1).

Eqs. (9) and (10) were proposed from considering the part of the N -particle wave function which was removed. However, when we consider subsequent absorptions, care must be taken to avoid double counting. A part of the absorbed wave is, via the source term, Eq. (12), transferred to the $(N-1)$ -particle sub-system. This part may go on to be absorbed within this sub-system, and, correspondingly, it will contribute to

the differential probability obtained from ρ_{N-1} , cf. Eq. (11). Eq. (13) must be modified accordingly; the term

$$\langle \varphi_\varepsilon | \mathcal{S}[\rho_N] | \varphi_\varepsilon \rangle, \quad (14)$$

must be removed from the right hand side. As explained in App. A, this contribution coincides with the last term in Eq. (13). After having removed it, we integrate the remaining expression over time and arrive at the following formula for the ε -differential probability distribution of the first particle to undergo absorption from the two-particle system:

$$\frac{\partial P_2}{\partial \varepsilon} = \frac{2}{\hbar} \int \int \varphi_\varepsilon^*(x) \varphi_\varepsilon(x') \times \{\gamma(x) + \gamma(x')\} \Phi(x, x') dx dx', \quad (15)$$

where

$$\Phi(x, x') = \int_0^\infty \int \Psi_2(x, y; t) \Psi_2^*(x', y; t) dy dt. \quad (16)$$

Here, Φ amounts to an effective time-integrated one-particle density matrix. This “density matrix” is weighted by the CAP function for each of the two variables, these terms are then added and projected onto the scattering states of interest.

While the wave function $|\Psi_2\rangle$ vanish as the first particle is absorbed, we may continue to simulate the dynamics of the remaining one. This one-particle sub-system, which is described by the density matrix ρ_1 , follows Eq. (11) with $n = 1$. As we are dealing with a one-particle system in this case, the diagonal matrix element in Eq. (10) coincides with that of Eq. (9):

$$\hbar \frac{d}{dt} \frac{\partial P_1}{\partial \varepsilon} = \langle \varphi_\varepsilon | \{\Gamma, \rho_1\} | \varphi_\varepsilon \rangle. \quad (17)$$

With only one remaining particle, nothing needs to be removed in order to avoid double counting. The resulting differential probability for the second absorption event reads

$$\frac{\partial P_1}{\partial \varepsilon} = \frac{1}{\hbar} \int \int \varphi_\varepsilon^*(x) \varphi_\varepsilon(x') \times \{\gamma(x) + \gamma(x')\} \int_0^\infty \rho_1(x, x'; t) dt dx dx', \quad (18)$$

see App. A for details. Note that Eq. (18) coincides with Eq. (15) if we substitute the time-integral of ρ_1 with 2Φ .

In Eqs. (15) and (18) we have analysed the absorbed wave by projection onto time-independent scattering states. When the quantity in question, ε , bears explicit time-dependence, obtaining converged results may require time-dependent scattering states, in which case Eqs. (15, 18) must be modified to

$$\frac{\partial P_2}{\partial \varepsilon} = \frac{2}{\hbar} \int_0^\infty \int \int \varphi_\varepsilon^*(x; t) \varphi_\varepsilon(x'; t) \{\gamma(x) + \gamma(x')\} \times \int \Psi_2(x, y; t) \Psi_2(x', y; t)^* dy dx dx' dt. \quad (19)$$

and

$$\frac{\partial P_1}{\partial \varepsilon} = \frac{1}{\hbar} \int_0^\infty \int \int \varphi_\varepsilon^*(x; t) \varphi_\varepsilon(x'; t) \times \{\gamma(x) + \gamma(x')\} \rho_1(x, x'; t) dx dx' dt, \quad (20)$$

respectively. This is somewhat analogous to what is done within the *time-dependent surface flux method* and in the *mask method*, in which photo electron spectra are calculated during the interaction with an external electric field by projection onto Volkov states, i.e., the eigen-states of the Hamiltonian for a free particle exposed to electromagnetic radiation, see, e.g., [5, 20, 26, 27, 29, 54].

III. NUMERICAL EXAMPLES

We will consider two examples here, both of which involve two interacting particles in one-dimension. The first one, which is without explicit time dependence in the Hamiltonian, addresses a scattering event which could be realized in a quantum dot with narrow confinement in two orthogonal directions. The second addresses a system trapped in the ground state of a confining potential exposed to a pulse of electromagnetic radiation. It may serve as a model for photo ionization of an atom with two active electrons. In both cases, the two-particle Hamiltonian may be written

$$H_{\text{eff}} = h_{\text{eff}}^{(1)} + h_{\text{eff}}^{(2)} + W \quad (21)$$

where the one-particle Hamiltonians $h_{\text{eff}}^{(i)}$ contain a time-independent, Hermitian part, h_0 , the CAP and, possibly, a time-dependent perturbation. The particles interact via a regularized Coulomb potential:

$$W(x_{12}) = \frac{W_0}{\sqrt{x_{12} + s^2}}, \quad (22)$$

where $x_{12} = |x_1 - x_2|$ and s is a smoothness parameter. We have chosen to use a square CAP function,

$$\gamma(x) = \begin{cases} \gamma_0(|x| - x_0)^2, & |x| \geq x_0 \\ 0, & |x| < x_0 \end{cases}, \quad (23)$$

where x_0 defines the onset of the CAP region.

Here and in the reminder of the paper, “ x ” refers exclusively to the position variable, and our dynamical variable of interest, ε , will be energy. In both examples we will deal with states which are symmetric under exchange of the spatial variables, which corresponds to a spin singlet state for fermions. Thus, these particles are, formally, bosons in this context.

Before presenting numerical results, we briefly outline how the calculations are implemented.

A. The implementation

The time evolution of the two-particle system, i.e., the solution of Eq. (4), is obtained by a second order split operator technique [55]. The implementation is facilitated by

expressing the two particle wave function $\Psi_2(x_1, x_2; t) = \langle x_1, x_2 | \Psi_2(t) \rangle$, where $|x_1, x_2\rangle$ is a product state, in terms of a matrix. This way, the action of the one-particle parts of the Hamiltonian, $h_{\text{eff}}^{(1)}$ and $h_{\text{eff}}^{(2)}$, corresponds to left and right multiplication, respectively, while the action of the particle-interaction, $W\Psi_2(t)$, corresponds to elementwise multiplication (Hadamard product). The momentum operator is represented by means of the fast Fourier transform (FFT).

The evolution of the one-particle sub-system follows Eq. (11) with $n = 1$:

$$i\hbar \frac{d}{dt} \rho_1 = h_{\text{eff}} \rho_1 - \rho_1 h_{\text{eff}}^\dagger + 2i\mathcal{S}[\Psi_2] \langle \Psi_2 \rangle \langle \Psi_2 \rangle. \quad (24)$$

In our matrix formulation, the last term above, the source term, may be calculated as

$$S = 4h\Psi_2(t)D\Psi_2^\dagger(t), \quad (25)$$

where the diagonal matrix $D = \text{diag}(\gamma(\mathbf{x}))$ is the CAP, and h is the step size used in the spatial discretization.

Also for ρ_1 , the scheme used for the time evolution is of second order in the numerical time step. The evolution dictated by the first two terms on the right hand side of Eq. (24) may be achieved by means analogous to the one-particle part of the propagator for the two-particle pure state. The propagator also features terms originating directly from the source term and cross-terms between the source term and the effective Hamiltonian. See App. B for more detail.

We have also calculated the time-dependent zero-particle probability p_0 , which is obtained from Eq. (11) by simply time-integrating the source term $\mathcal{S}[\rho_1(t)]$, which is a scalar. While this does not provide any differential information about any absorbed particles, it serves as a useful check for the numerics. The Lindblad equation ensures that the trace of the total density matrix remains unity. In this context, this means that

$$|\Psi_2(t)|^2 + \text{Tr}\rho_1(t) + p_0(t) = 1 \quad (26)$$

at all times. As our numerical scheme is not manifestly trace conserving, the deviation from unity serves as a measure of the accuracy of simulations.

In our examples, we set out to calculate the energy distribution of the unbound particles emerging after interaction. We do so by projection onto the eigen-states of the unperturbed, Hermitian one-particle Hamiltonian h_0 as dictated by Eqs. (15,18). With our matrix representation of the two-particle wave function, the spatial integral in Eq. (16) may be found by matrix multiplication. Numerically, the effective one-particle density matrix of Eq. (16) may be calculated as a sum of matrix products,

$$\Phi = h\tau \sum_{t_n} \Psi_2(t_n) \Psi_2^\dagger(t_n), \quad (27)$$

where τ is the temporal step size. Eq. (15) may conveniently be expressed as

$$\hbar \frac{\partial P_2}{\partial \varepsilon} \approx 2h^2 \varphi_\varepsilon^\dagger (D\Phi + \Phi D) \varphi_\varepsilon, \quad (28)$$

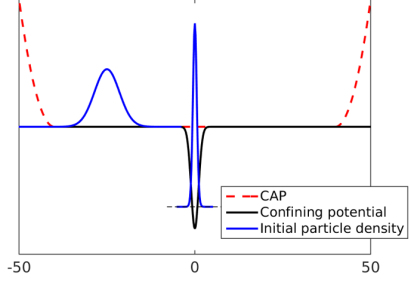


FIG. 1: The figure illustrates the situation prior to collision. A projectile particle of rather sharply defined initial momentum is incident upon a target particle initially trapped in the ground state of a confining potential.

where φ_ε represents the scattering state according to the eigen energy ε as a column vector. The ε -differential distribution obtained from ρ_1 is calculated analogously to Eq. (28) – with 2Φ replaced by the time-integral of ρ_1 . All in all, calculating the effective one-particle density matrix Φ when solving Eq. (4) and the time-integral of ρ_1 when solving Eq. (24) impose little extra numerical effort, apart from certain increase in memory requirements. Nor does acquiring the time-independent one-particle scattering states φ_ε impose any substantial numerical effort. We use the box-normalized eigenstates of the numerical unperturbed one-particle Hamiltonian h_0 in order to interpolate the continuous energy distribution – distinguishing between symmetric and anti-symmetric continuum states.

B. Example I: Scattering

In this example a target particle is initially trapped in the ground state of a short-ranged Gaussian potential,

$$V(x) = -V_0 \exp\left(-\frac{x^2}{2\sigma_V^2}\right), \quad (29)$$

while an identical projectile particle with a Gaussian wave packet is incident on the target, see Fig. 1. The situation could correspond to a quantum dot embedded in a quantum wire [49, 56–59].

We take our units to be defined by setting \hbar and the particle mass to unity. The confining potential has the strength $V_0 = 4$ and the width $\sigma_V = 3/(2\sqrt{2})$ in these units, cf. Eq. (29). This leads to a one-particle ground state energy of -3.141 . The interaction strength $W_0 = 1$, and for the softening parameter s , the value 0.1925 has been used, cf. Eq. (22). The square CAP function is nonzero for $|x|$ beyond $x_0 = 35$, cf. Eq. (23). The initial Gaussian projectile wave function is centred at $x = -20$ in position space and $p = 2$ in momentum space. Its momentum width is 0.1 , which corresponds to a position width of 5 length units.

Since the initial energy of the projectile is such that it does not allow for both particles to be liberated, it suffices to solve Eq. (4); we do not need to consider any second absorption.

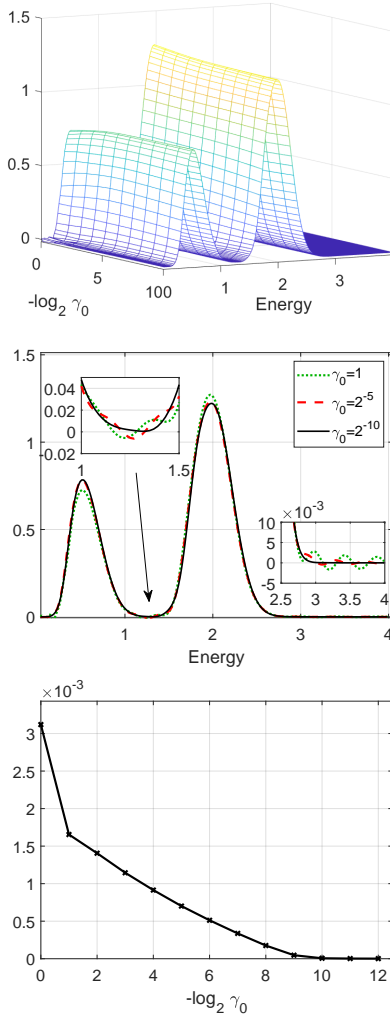


FIG. 2: *Upper panel:* The energy spectrum of the unbound particle emerging from the collision event. In this case, the projectile particle has an initial mean momentum of 2 units and the target particle is trapped in the ground state with energy -3.14 units. The spectrum is predicted by Eq. (15) and calculated for various values of the strength of the CAP function, i.e., γ_0 in Eq. (23). *Middle panel:* The same distribution as in the upper panel for three values of γ_0 . The inserts display close-ups on regions in which un converged spectra feature negative values. *Lower panel:* In this plot, the total negative contribution to the (un converged) energy distributions is plotted as a function of absorber strength.

The upper panel of Fig. 2 shows the energy distribution of the particle emerging from the collision event as predicted by Eq. (15). In addition to energy, it is also shown as a function of the CAP strength γ_0 , cf. Eq. (23). This parameter is chosen such that $\gamma_0 = 2^{-n}$ where n is a non-negative integer. We see that not only does the distribution converge as γ_0 decreases; it is in fact virtually independent of γ_0 . Only for very strong absorption can we see deviations from the converged one.

In the middle panel of Fig. 2, the same energy spectra are shown for three values of γ_0 . We see that the wave emerging from the collision event comes up in two energy lobes. This

is due to the fact that the target has, with a certain probability, been excited in the event. In other words, the peak centred around 2 energy units corresponds to elastic scattering while the peak near 0.5 energy units corresponds to inelastic scattering.

The inserts in the panel reveal that the spectra obtained with comparatively hard absorption are not strictly non-negative; in certain regions they are negative. This is related to the fact that, as discussed in Sec. II A, the operator $\{\Gamma, \rho_N\}$ in Eqs. (9) and (10) is not necessarily positive semi-definite. Thus, there is no mathematical reason why differential quantities obtained from Eq. (15) must be non-negative. However, in the limit $\gamma_0 \rightarrow 0^+$, when the predictions become physical, no negative parts are seen. This is demonstrated more explicitly in the lower panel of Fig. 2, which depicts the unphysical negative contribution to the energy distribution $\partial P_2 / \partial \varepsilon$,

$$-\int_{\partial P_2 / \partial \varepsilon < 0} \frac{\partial P_2}{\partial \varepsilon} d\varepsilon, \quad (30)$$

as a function of γ_0 . We clearly see that this undesirable feature in fact vanishes for finite values of γ_0 .

In order to reduce the necessary grid size, it is desirable to use as hard absorption as possible – while still obtaining converged spectra and avoiding artificial reflections. In Fig. 3 we display how the extension of the wave function, which is subjected to absorption, and the duration of the simulation depends on the strength of the absorber. We have here defined the former as the smallest a which is such that whatever resides beyond $|x| = a$ has a squared norm less than 1 % throughout the simulation. The duration we have defined as the time it takes $|\Psi_2(t)|^2$ to fall below 1 %. The left panel shows, as expected, that a larger grid is necessary as the CAP strength is reduced. When it comes to the duration of the simulation, however, the behaviour is not monotonous; initially, the time it takes to simulate the entire event actually decreases with decreasing γ_0 . This is due to artificial reflections induced by too hard absorption. Reflected waves will have to travel back across the grid at least one more time before being absorbed, and, thus, complete absorption takes longer in this case.

In Fig. 4 we display the results of a collision event for which the liberation of both particles is energetically admissible. In this case the projectile particle has an initial momentum with a mean value of 3.5 units and a width of 0.2 units. The left panel of Fig. 4 reveals that elastic scattering is the dominant process. However, as the right panel shows, there is a certain probability for the second particle to be liberated as well. The corresponding energy distribution is obtained from Eq. (18), which, in turn, requires the solution of Eq. (24) in addition to Eq. (4). It is seen that this second particle predominantly comes out with low energy. It is also seen that also this energy distribution is very weakly dependent on γ_0 . We do see some dependence, however, close to threshold. This is related to the fact that particles with near-zero energy require a very long time to reach the absorber; complete absorption is hard to achieve in a simulation of finite duration in this case. It may seem counter-intuitive that this issue is more prominent at harder absorption than softer absorption. It can be understood

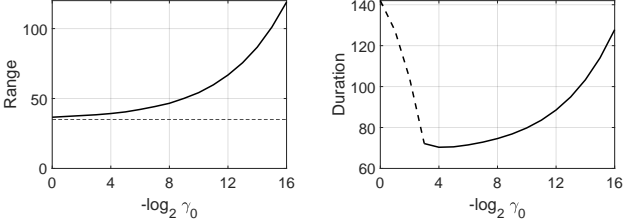


FIG. 3: These panels show the maximum range of the wave function (left) and the duration of the simulation (right) for the collision example pertaining to Fig. 2. For the sake of illustration, we have included calculations featuring much weaker absorption than necessary. The horizontal dashed line in the left panel indicates the onset of the CAP function, and the dashed part of the curve in the right panel indicates the region in which artificial reflection effectively prolongs the simulations.

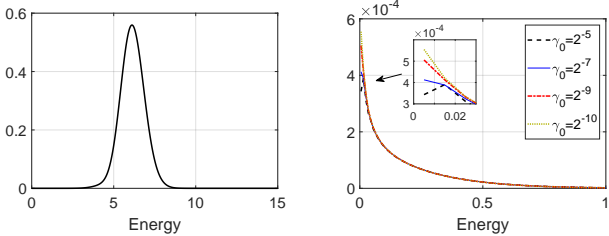


FIG. 4: The left panel, which is analogous to the middle panel of Fig. 2, shows the energy distribution of the first particle to be absorbed after collision. Here the mean momentum of the projectile particle is 3.5 units, and its width is 0.2. The right panel displays the energy distribution of the second particle to be absorbed. As this distribution integrates to a rather low total probability, it is not likely that two liberated particles will emerge from the collision. The distribution in the right panel features a certain dependence of the strength of the CAP function, γ_0 in Eq. (23), near threshold. No such dependence can be made out for these values of γ_0 in the left panel.

from what we saw in the right panel of Fig. 3. Low-energy waves are more prone to be reflected by the CAP than faster ones – and increasingly so with harder absorption. Consequently, with a finite duration of simulations, 1000 time units in this case, the slow, reflected waves do not have enough time to hit the absorber many enough times to reach full absorption.

C. Example II: Photo ionization

The next example addresses a model for photo ionization of a two-electron atom. The electrons are initially confined in the two-particle ground state of a regularized Coulomb potential with a functional form identical to the interaction Eq. (22):

$$V(x) = \frac{V_0}{\sqrt{x^2 + u^2}}. \quad (31)$$

Numerically, this initial state is constructed by evolving the system without the CAP in *imaginary time*, i.e., by substituting t with $-it$ in Eq. (4) with $\Gamma = 0$. This, along with renormalization at each time step, causes virtually any initial state

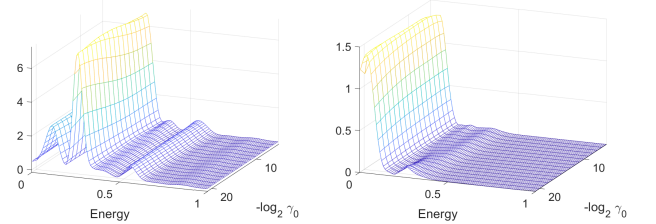


FIG. 5: These plots show the photo electron spectra for a model two-electron atom exposed to a laser pulse. The spectra are calculated with various absorber strengths, i.e., γ_0 in Eq. (23). The left panels are obtained from absorption from the original two-particle system, while the right panels are obtained from the one-particle sub-system which remains after the first absorption event.

to converge towards the ground state exponentially. Next, the system is exposed to a laser pulse. The interaction is formulated in the velocity gauge, i.e., the Hermitian part of the one-particle hamiltonian reads

$$h_i = \frac{p_i^2}{2m} + V(x_i) + \frac{e}{m} A(t) p_i, \quad (32)$$

where $i = 1, 2$ refers to the particle number, m is the electron's mass and $-e$ is its charge. The homogeneous vector potential A reads

$$A(t) = \begin{cases} \frac{E_0}{\omega} \sin^2 \left(\frac{\pi}{T} \omega t \right) \sin(\omega t), & 0 \leq t \leq T \\ 0, & \text{otherwise} \end{cases}. \quad (33)$$

In this particular example we apply atomic units, a.u., which may be defined by, in addition to setting \hbar and m to unity as in Sec. III B, choosing the elementary charge e and the Bohr radius as units for their respective quantities. Here, the peak electric field strength is $E_0 = 0.1$ a.u., the central angular frequency ω is 0.3 a.u., and the duration T corresponds to seven optical cycles. The confining potential, Eq. (31), is chosen such that both V_0 and u are 0.5 a.u.. This yields a one-particle ground state energy of $-1/2$ a.u.. The interaction, Eq. (22), has strength $W_0 = 0.5$ a.u., while the interaction smoothness is the same as for the confining potential; $s = u = 0.5$ a.u.. This gives a two-particle ground state energy of -0.554 a.u.. Thus, one particle is rather weakly bound. The CAP is turned on at $|x| = x_0 = 50$ atomic length units.

Figure 5 demonstrates, analogously to the upper panel of Fig. 2, how the predicted singly-differential photo-electron spectra depend on the strength of the CAP function. The left panel is the spectrum obtained from the first absorption, calculated using Eq. (15), and the right one corresponds to the second absorption, calculated using Eq. (18). The spectrum obtained from the first absorption is not as close to being γ_0 -independent as the one in Fig. (2). We can, e.g., detect a slight shift towards higher energies as γ_0 approaches zero. However, the dependence on the CAP strength is still quite weak, and the spectrum does converge rather rapidly as the CAP strength diminishes.

Interestingly, this happens in spite of the fact that much of the absorption takes place during interaction with the laser

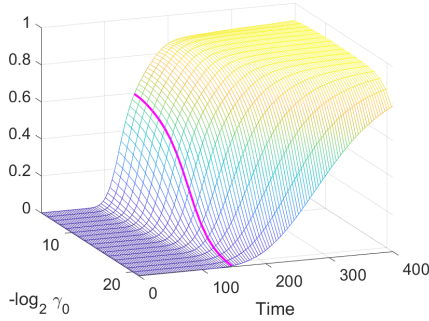


FIG. 6: The total absorption from the two-particle system, $1 - |\Psi_2(t)|^2$, as a function of time and absorber strength γ_0 . The thick, purple curve indicates the time at which the laser pulse is over.

pulse. This is illustrated in Fig. (6), which depicts the depletion in norm from Ψ_2 as a function of time, i.e., it shows $1 - |\Psi_2(t)|^2$ as a function of t and γ_0 . The thick purple curve corresponds to the time at which the pulse is switched off. By comparing Fig. 6 with the left panel of Fig. 5 it is seen that a converged spectrum is obtained before the laser interaction is over. Due to the corresponding explicit time-dependence in the Hamiltonian, it would seem more reasonable to apply Eq. (19), which involves time-dependent scattering states, rather than Eq. (15). And even doing so, you would still deprive an electron the possibility to exchange energy with the laser field when it is absorbed during interaction. The latter can only mean that such exchange predominantly takes place within the CAP free region. The fact that Eq. (15), in which the absorbed wave is projected onto time-independent scattering states, indeed produces a converged spectrum during interaction is related to the fact that the interaction is described in the velocity gauge. In this formulation, a free, classical electron is at rest in momentum space; the momentum is a constant of motion. This is reflected in the fact that the free-electron Volkov solutions are time-independent – apart from a phase factor which does not contribute in this formalism. In fact, if we substitute our scattering states φ_ε with solutions in which the confining potential is removed, i.e., plane waves, we would obtain a similar spectrum – except for a shift towards higher energies due to the neglect of the Coulomb-like potential.

While the energy distribution of the first electron to be absorbed, $\partial P_2/\partial \varepsilon$, converges rather quickly as the CAP strength is reduced, this is not the case for the second particle to be absorbed. The right panel of Fig. 5 shows $\partial P_1/\partial \varepsilon$ obtained from Eq. (18). Although the first peak near threshold is rather well resolved, the next peak, centred near $\varepsilon = 0.25$ a.u., reveals a rather slow convergence. Fig. 7, which shows the same spectra as in Fig. 5 on a semi-logarithmic plot for certain values of γ_0 , shows more details in this regard. The spectrum of the first absorbed particle, $\partial P_2/\partial \varepsilon$, features several well converged multi-photon peaks. The spectra obtained from the second absorption, $\partial P_1/\partial \varepsilon$, features a γ_0 -dependence which seems to increase with increasing energy.

Figure 8 shows the same as Fig. 7 – however with the cen-

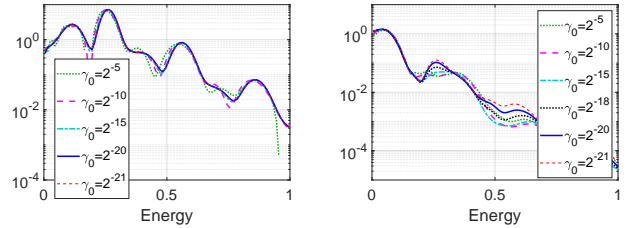


FIG. 7: These plots show the same photo electron spectra as in Fig. 5 for certain values of the CAP strength, however using a logarithmic y -axis. As in Fig. 5, the left panel stems from the first absorption while the right one is calculated from the second absorption. The green curve, which corresponds to rather strong absorption, is seen to vanish for in certain energy intervals in the left panel. This is because too strong absorption may induce negative values for the spectrum, cf. the lower panel of Fig. 30.

tral laser frequency $\omega = 1$ a.u.. This allows for one-photon double ionization, as opposed to the previous case. Here, the onset of the CAP region is at $x_0 = 20$ a.u.. The same patterns as in Fig. 7 are seen. $\partial P_2/\partial \varepsilon$ becomes virtually γ_0 -independent at comparatively strong absorption, while it takes a lower γ_0 -value for $\partial P_1/\partial \varepsilon$ to converge – in particular at higher energies. The price to pay for weak absorption is the need for a larger numerical domain, cf. Fig. 3. For the case of Fig. 8, the weakest absorption required a grid extending from -362 a.u. to 362 a.u. – for each particle. This is, of course, still far less than the actual extension of the wave function by the time all of the unbound part has left the interaction region. The results of Figs. 7 and 8 are consistent with the bias introduced in the sequential double absorption process: The fastest electron reaches the absorber first. In situations such as these ones, in which both electrons of Ψ_2 may have reached the continuum simultaneously, the most energetic of the two would predominantly contribute to the $\partial P_2/\partial \varepsilon$ -spectrum, which, in turn, causes slower electrons to be overrepresented, so to speak, in $\partial P_1/\partial \varepsilon$. As the CAP strength decreases, so does this bias. And for a γ_0 -independent spectrum, the singly differential $\partial P_1/\partial \varepsilon$ spectrum may be interpreted as the integrated doubly differential double ionization spectrum,

$$\frac{\partial P_1}{\partial \varepsilon} \xrightarrow{\gamma_0 \rightarrow 0^+} \int_0^\infty \frac{\partial^2 P_{\text{double}}}{\partial \varepsilon \partial \varepsilon'} d\varepsilon'. \quad (34)$$

From this point of view, it is not surprising that the multi-photon peaks seen in $\partial P_1/\partial \varepsilon$, i.e. the left panels of Figs. 7 and 8 are less pronounced than the ones seen in $\partial P_2/\partial \varepsilon$, i.e. the right panels.

While the bias inherent in the sequential nature of the scheme presented here may be undesirable in many situations, it may be of interest in others. For instance, the situation does resemble an experimental situation in the sense that liberated particles are detected one-by-one – and the most energetic ones first. The similarity between CAPs and detectors, see, e.g., [9, 52], could facilitate comparison with experiment.

It is worth while to also address *total* ionization probabilities in this context. The converged spectrum obtained from

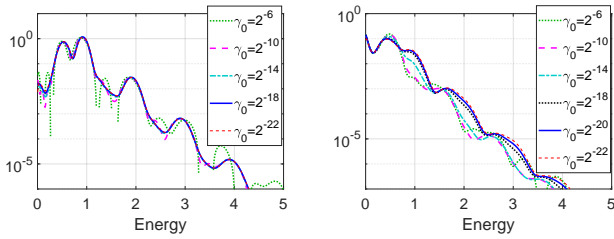


FIG. 8: These plots show the kind of photo electron spectra as in Fig. 8 – however with $\omega = 1$ a.u. in this case, cf. Eq. (33). Here, the CAP function sets on at $x_0 = 20$ a.u.. The left panel corresponds to the predictions of Eq. (15), while the right panel is obtained using Eq. (18).

absorbing an electron from the two-particle wave function, $\partial P_2 / \partial \varepsilon$, integrates to the total norm loss from Ψ_2 . In the case of Fig. 6 we see that this probability is close to one. Actually, the integral of $\partial P_2 / \partial \varepsilon$ is slightly less than the total absorption because we in Eq. (15) have only projected onto scattering states corresponding to positive (one-particle) energies. This enables us to avoid artificial contributions to the ionization probability from populations in Rydberg states which overlap with the CAP. The ionization probability

$$P_2 = \int_0^\infty \frac{\partial P_2}{\partial \varepsilon} d\varepsilon \quad (35)$$

is indeed *total* in the sense that it includes both single and double ionization; the spectrum $\partial P_2 / \partial \varepsilon$ is the energy differential probability distribution of the photo electron which is absorbed first – irrespective of whether also the second electron goes on to be ionized as well or not. Thus, $\partial P_2 / \partial \varepsilon$ cannot be interpreted as the spectrum of the photo electron emerging from single ionization alone – unless the probability of double ionization is negligible compared to single ionization. The converged difference between this spectrum and $\partial P_1 / \partial \varepsilon$, however, would correspond to the single ionization event exclusively.

The spectrum $\partial P_1 / \partial \varepsilon$ in Eq. (18) is calculated from the second absorption and, correspondingly, integrates to the double ionization probability. Note that this quantity,

$$P_1 = \int_0^\infty \frac{\partial P_1}{\partial \varepsilon} d\varepsilon, \quad (36)$$

is not subject to the same γ_0 -dependence as is the spectrum $\partial P_1 / \partial \varepsilon$. P_1 is the probability of double absorption irrespective of the bias addressed above. Again, P_1 tends to be somewhat lower than the final population of the vacuum state, $p_0(t \rightarrow \infty)$, due to the possible population of Rydberg states. In this respect, it should be mentioned that Rydberg populations in the two-particle system could lead to an undesired population of the one-particle sub-system. Our numerical studies have, however, not shown any indication of this affecting the $\partial P_1 / \partial \varepsilon$ -distribution.

D. Concluding remarks

The scheme presented in these numerical examples involves solving a non-Hermitian two-particle Schrödinger equation and a one-particle master equation with a source term. The complexity involved in each of them is comparable. The calculation of the energy-resolved spectra does not impose any significant complication in terms of implementation nor computational resources. Of course, there are several situations in which Eq. (15) or Eq. (19), which only requires the solution of Eq. (4), provides interesting and relevant results without the need to resolve the spectrum provided by Eq. (18) or Eq. (20), which also requires the solution of Eq. (24). It is also worth noting that the formalism may fruitfully be applied to one-particle systems as well.

We have seen that rather weak CAPs may be necessary in order to obtain well resolved energy spectra. We have, however, not given any attention to how the *shape* of the CAP function affects this convergence. It would be quite interesting to study whether other choices of CAP functions than Eq. (23), or other CAPs than local ones, could provide faster convergence. This is a topic which merits further investigation. Such an investigation should also aim at formulating precise and general convergence criteria.

Another interesting question in this regard is whether absorption after explicitly time-dependent interactions could be treated or, at least, facilitated by analytical means, thus evading comparatively time-consuming simulations. In this regard, the works of Refs. [24, 32] are inspirational. While these issues are beyond the scope of the present work, they will be subject to further investigation.

IV. CONCLUSIONS

We have presented an approach to unbound multi-particle quantum dynamics which allows us to impose absorbing boundary conditions and yet calculate the probability distributions of interest for all of the absorbed particles. It does so by using a complex absorbing potential which, in addition to removing the outgoing, unbound parts of the wave function, also *probe* them. The fact that the absorber is a one-particle operator allows us to analyse the unbound part by projecting onto single-particle scattering states – as opposed to many-particle scattering states. This, in turn, enables rather straight forward implementation. It also provides a conceptually transparent approach which, via the Lindblad equation, generalizes naturally to any number of particles.

The applicability of the scheme was demonstrated by calculating energy spectra for two examples featuring two-particle models – one example involving scattering and another involving photo ionization. In the latter case, it was seen that the spectrum originating from the first absorption converged faster than the one obtained from the second absorption in terms of the absorber strength.

Acknowledgements

This work has benefited from valuable input from dr. S. Carlström, prof. S. Denysov and dr. S. Kvaal.

Appendix A: Derivation of the formulas for differential probabilities

Here we derive the differential probability distribution for absorption from a two and one particle system, Eq. (15) and Eq. (18), respectively, from the more general form of Eq. (10). In doing so, we express both operators, density matrices and state vectors by means of second quantization. The fermionic two-particle wave function is written

$$\begin{aligned} |\Psi_2\rangle &= \int \int \Psi_2(x_1, x_2) |x_1, x_2\rangle dx_1 dx_2 = & (A1) \\ &\frac{1}{\sqrt{2}} \int \int \Psi_2(x_1, x_2) |\{x_1, x_2\}\rangle dx_1 dx_2 = \\ &\frac{1}{\sqrt{2}} \int \int \Psi_2(x_1, x_2) \hat{\psi}^\dagger(x_1) \hat{\psi}^\dagger(x_2) |-\rangle dx_1 dx_2, \end{aligned}$$

where $|x_1, x_2\rangle$ is a product basis state, $|\{x_1, x_2\}\rangle$ is a properly anti-symmetrized one and $|-\rangle$ is the vacuum state, i.e., the state in which there are no particles. The two-particle wave function is anti-symmetric with respect to exchange,

$$\Psi_2(x_1, x_2) = -\Psi_2(x_2, x_1). \quad (A2)$$

We also express the one-particle density matrix and the scattering states by means of second quantization:

$$\begin{aligned} \rho_1 &= \int \int \rho_1(x, x') |x\rangle \langle x'| dx dx' = \\ &\int \int \rho_1(x, x') \hat{\psi}^\dagger(x) |-\rangle \langle -| \hat{\psi}(x') dx dx' \quad (A3) \end{aligned}$$

and

$$|\varphi_\varepsilon\rangle = \int dx \varphi_\varepsilon(x) \hat{\psi}^\dagger(x) |-\rangle. \quad (A4)$$

We start by writing out Eq. (10) for $N = 2$ explicitly. With Eqs. (2, A1, A3, A4), it reads

$$\begin{aligned} \hbar \frac{d}{dt} \frac{\partial P}{\partial \varepsilon} &= \int dx \langle \varphi_\varepsilon | \hat{\psi}(x) \{ \Gamma, |\Psi_2\rangle \langle \Psi_2| \} \hat{\psi}^\dagger(x) | \varphi_\varepsilon \rangle = \\ &\Re \int dx \int dy \int dx' \int \int dx_1 dx_2 \varphi_\varepsilon^*(y) \gamma(x') \Psi_2(x_1, x_2) \\ &\times \langle -| \hat{\psi}(y) \hat{\psi}(x) \hat{\psi}^\dagger(x') \hat{\psi}^\dagger(x') \hat{\psi}^\dagger(x_1) \hat{\psi}^\dagger(x_2) | -\rangle \\ &\times \int \int dx'_1 dx'_2 \int dy' \Psi_2^*(x'_1, x'_2) \varphi_\varepsilon(y') \\ &\times \langle -| \hat{\psi}(x'_2) \hat{\psi}(x'_1) \hat{\psi}^\dagger(x) \hat{\psi}^\dagger(y') | -\rangle. \end{aligned}$$

The vacuum matrix elements may be found, e.g., by using Wick's theorem [60]:

$$\begin{aligned} \langle -| \hat{\psi}(y) \hat{\psi}(x) \hat{\psi}^\dagger(x') \hat{\psi}(x') \hat{\psi}^\dagger(x_1) \hat{\psi}^\dagger(x_2) | -\rangle &= \\ &\delta(y - x') [\delta(x - x_1) \delta(x' - x_2) - \delta(x - x_2) \delta(x' - x_1)] \\ &- \delta(x - x') [\delta(y - x_1) \delta(x' - x_2) - \delta(y - x_2) \delta(x' - x_1)] \end{aligned}$$

and

$$\begin{aligned} \langle -| \hat{\psi}(x'_2) \hat{\psi}(x'_1) \hat{\psi}^\dagger(x) \hat{\psi}^\dagger(y') | -\rangle &= \\ &\delta(x'_2 - y') \delta(x'_1 - x) - \delta(x'_2 - x) \delta(x'_1 - y'). \end{aligned}$$

With this and the exchange anti-symmetry of the two-particle wave function, Eq. (A2), we arrive at Eq. (13).

As explained in Sec. II, when we analyze the part which has been removed from $|\Psi_2\rangle$, we must make sure to remove the part which is reconstructed within ρ_1 in order to avoid double counting. This contribution is provided by the source term Eq. (12). The part to be removed from Eq. (13) is

$$\langle \varphi_\varepsilon | \mathcal{S}[\rho_2] | \varphi_\varepsilon \rangle$$

whith $\rho_2 = |\Psi_2\rangle \langle \Psi_2|$. Using Eqs. (12, A1, A4) it may be expressed as

$$\begin{aligned} 2 \langle \varphi_\varepsilon | \int dx \gamma(x) \hat{\psi}(x) | \Psi_2 \rangle \langle \Psi_2 | \hat{\psi}^\dagger(x) | \varphi_\varepsilon \rangle &= \\ &\int dy \varphi_\varepsilon(y) \int dx \gamma(x) \int \int dx_1 dx_2 \Psi_2(x_1, x_2) \\ &\times \langle -| \hat{\psi}(y) \hat{\psi}(x) \hat{\psi}^\dagger(x_1) \hat{\psi}^\dagger(x_2) | -\rangle \\ &\times \int dy' \int \int dx'_1 dx'_2 \varphi_\varepsilon(y') \Psi_2^*(x'_1, x'_2) \\ &\times \langle -| \hat{\psi}(x'_2) \hat{\psi}(x'_1) \hat{\psi}^\dagger(x) \hat{\psi}^\dagger(y') | -\rangle. \end{aligned}$$

The repeated vacuum matrix element is

$$\begin{aligned} \langle -| \hat{\psi}(y) \hat{\psi}(x) \hat{\psi}^\dagger(x_1) \hat{\psi}^\dagger(x_2) | -\rangle &= \\ &\delta(y - x_2) \delta(x - x_1) - \delta(y - x_1) \delta(x' - x_2). \end{aligned}$$

With this and the exchange anti-symmetry of the two-particle wave function we arrive at

$$\begin{aligned} \langle \varphi_\varepsilon | \mathcal{S}[\rho_2] | \varphi_\varepsilon \rangle &= \\ &\int dx \gamma(x) \int dy \varphi_\varepsilon^*(y) 2 \Psi_2(x, y) \int dy' \varphi_\varepsilon(y) 2 \Psi_2^*(x, y') = \\ &4 \int dx \gamma(x) \left| \int dy \varphi_\varepsilon^*(y) \Psi_2(x, y) \right|^2. \end{aligned}$$

This coincides the last term in Eq. (13), which, accordingly, is to be removed.

Appendix B: A propagator for the one-particle density matrix

A second order Taylor expansion of $\rho_1(t)$ in time says that

$$\rho_1(t + \tau) = \rho_1 + \tau \dot{\rho}_1 + \frac{1}{2} \tau^2 \ddot{\rho}_1 + \mathcal{O}(\tau^3). \quad (B1)$$

Here, the dots indicate time-derivatives and, for convenience, the absence of an argument is to be interpreted as “ (t) ”. $\dot{\rho}_1$

and $\ddot{\rho}_1$ are provided by Eq. (24) and its time derivative, respectively. If we write them out explicitly, Eq. (B1) reads

$$\begin{aligned} \rho_1(t + \tau) = & \rho_1 - i \frac{\tau}{\hbar} \left(h_{\text{eff}} \rho_1 - \rho_1 h_{\text{eff}}^\dagger + i \mathcal{S}[\Psi_2] \right) \\ & + \frac{\tau^2}{2\hbar^2} \left(\left(-i\hbar \dot{h}_{\text{eff}} - h_{\text{eff}}^2 \right) \rho_1 - \right. \\ & \left. \rho_1 \left(-i\hbar \dot{h}_{\text{eff}}^\dagger + (h_{\text{eff}}^\dagger)^2 \right) \right. \\ & \left. + 2h_{\text{eff}} \rho_1 h_{\text{eff}}^\dagger - i \left[h_{\text{eff}} \mathcal{S}[\Psi_2] - \mathcal{S}[\Psi_2] h_{\text{eff}}^\dagger \right] \right. \\ & \left. + \hbar \frac{d}{dt} \mathcal{S}[\Psi_2] \right) + \mathcal{O}(\tau^3), \end{aligned} \quad (\text{B2})$$

where h_{eff} is here the effective one-particle Hamiltonian. In an autonomous system, \dot{h}_{eff} vanishes and the scheme is somewhat simplified.

Now, the sum of the terms which do not contain source term contributions may, to third order in τ , be written as

$$\exp \left(-i \frac{\tau}{\hbar} h_{\text{eff}}(t + \tau/2) \right) \rho_1 \exp \left(i \frac{\tau}{\hbar} h_{\text{eff}}^\dagger(t + \tau/2) \right). \quad (\text{B3})$$

Moreover,

$$\begin{aligned} \frac{\tau}{\hbar} \mathcal{S}[\Psi_2] + \frac{\tau^2}{2\hbar} \frac{d}{dt} \mathcal{S}[\Psi_2] = & \\ \frac{\tau}{2\hbar} (\mathcal{S}[\Psi_2] + \mathcal{S}[\Psi_2(t + \tau)]) + \mathcal{O}(\tau^3), \end{aligned} \quad (\text{B4})$$

which allows for a convenient implementation simply by keeping the previous source term in memory.

All in all, we arrive at the following scheme:

$$\begin{aligned} \rho_1(t + \tau) = & e^{-i\tau/\hbar h_{\text{eff}}(t + \tau/2)} \rho_1(t) e^{i\tau/\hbar h_{\text{eff}}^\dagger(t + \tau/2)} \\ & + \frac{\tau}{2\hbar} (\mathcal{S}[\Psi_2(t)] + \mathcal{S}[\Psi_2(t + \tau)]) \\ & - i \frac{\tau^2}{2\hbar^2} \left[h_{\text{eff}}(t) \mathcal{S}[\Psi_2(t)] - \mathcal{S}[\Psi_2(t)] h_{\text{eff}}^\dagger(t) \right] + \mathcal{O}(\tau^3). \end{aligned} \quad (\text{B5})$$

[1] U. D. Giovannini, A. H. Larsen, and A. Rubio, *Eur. Phys. J.* **B88**, 56 (2015).
[2] C. W. McCurdy, M. Baertschy, and T. N. Rescigno, *J. Phys. B* **37**, R137 (2004).
[3] A. Scrinzi, H. Stimming, and N. Mauser, *J. Comput. Phys.* **269**, 98 (2014).
[4] J. L. Krause, K. J. Schafer, and K. C. Kulander, *Phys. Rev. A* **45**, 4998 (1992).
[5] S. Chelkowski, C. Foisy, and A. D. Bandrauk, *Phys. Rev. A* **57**, 1176 (1998).
[6] R. Grobe, S. Haan, and J. Eberly, *Comput. Phys. Commun.* **117**, 200 (1999).
[7] M. Lein, J. P. Marangos, and P. L. Knight, *Phys. Rev. A* **66**, 051404 (2002).
[8] V. Weisskopf and E. Wigner, *Zeit. Phys.* **63**, 54 (1930).
[9] R. Kosloff and D. Kosloff, *J. Comput. Phys.* **63**, 363 (1986).
[10] A. Scrinzi, *Phys. Rev. A* **81**, 053845 (2010).
[11] U. V. Riss and H. D. Meyer, *J. Phys. B* **26**, 4503 (1993).
[12] T. N. Rescigno, M. Baertschy, D. Byrum, and C. W. McCurdy, *Phys. Rev. A* **55**, 4253 (1997).
[13] N. Moiseyev, *J. Phys. B* **31**, 1431 (1998).
[14] D. E. Manolopoulos, *J. Chem. Phys.* **117**, 9552 (2002).
[15] R. Santra and L. S. Cederbaum, *Phys. Rep.* **368**, 1 (2002).
[16] J. Muga, J. Palao, B. Navarro, and I. Egusquiza, *Phys. Rep.* **395**, 357 (2004).
[17] Y. Sajeev, M. Sindelka, and N. Moiseyev, *Chem. Phys.* **329**, 307 (2006).
[18] G. Lindblad, *Comm. Math. Phys.* **48**, 119 (1976).
[19] V. Gorini, A. Kossakowski, and E. Sudarshan, *J. Math. Phys.* **17**, 821 (1976).
[20] A. M. Ermolaev, I. V. Puzynin, A. V. Selin, and S. I. Vinitsky, *Phys. Rev. A* **60**, 4831 (1999).
[21] A. M. Ermolaev and A. V. Selin, *Phys. Rev. A* **62**, 015401 (2000).
[22] M. Beck, A. Jäckle, G. Worth, and H.-D. Meyer, *Phys. Rep.* **324**, 1 (2000).
[23] B. Feuerstein and U. Thumm, *J. Phys. B* **36**, 707 (2003).
[24] A. Palacios, C. W. McCurdy, and T. N. Rescigno, *Phys. Rev. A* **76**, 043420 (2007).
[25] L. Greenman, P. J. Ho, S. Pabst, E. Kamarchik, D. A. Mazziotti, and R. Santra, *Phys. Rev. A* **82**, 023406 (2010).
[26] L. Tao and A. Scrinzi, *New J. Phys.* **14**, 013021 (2012).
[27] A. Scrinzi, *New J. Phys.* **14**, 085008 (2012).
[28] F. Yip, A. Palacios, T. Rescigno, C. McCurdy, and F. Martin, *Chemical Physics* **414**, 112 (2013).
[29] V. V. Serov, V. L. Derbov, T. A. Sergeeva, and S. I. Vinitsky, *Phys. Rev. A* **88**, 043403 (2013).
[30] A. Karamatskou, S. Pabst, Y.-J. Chen, and R. Santra, *Phys. Rev. A* **89**, 033415 (2014).
[31] V. P. Majety, A. Zielinski, and A. Scrinzi, *New J. Phys.* **17**, 063002 (2015).
[32] F. Morales, T. Bredtmann, and S. Patchkovskii, *J. Phys. B* **49**, 245001 (2016).
[33] X. Wang, J. Tian, and J. H. Eberly, *J. Phys. B* **51**, 084002 (2018).
[34] V. V. Serov, V. L. Derbov, B. B. Joulakian, and S. I. Vinitsky, *Phys. Rev. A* **63**, 062711 (2001).
[35] X. M. Tong, K. Hino, and N. Toshima, *Phys. Rev. A* **74**, 031405 (2006).
[36] A. Palacios, T. N. Rescigno, and C. W. McCurdy, *Phys. Rev. A* **77**, 032716 (2008).
[37] D. A. Horner, C. W. McCurdy, and T. N. Rescigno, *Phys. Rev. A* **78**, 043416 (2008).
[38] N. Rohringer and R. Santra, *Phys. Rev. A* **79**, 053402 (2009).
[39] A. Palacios, T. N. Rescigno, and C. W. McCurdy, *Phys. Rev. A* **79**, 033402 (2009).
[40] A. Palacios, D. A. Horner, T. N. Rescigno, and C. W. McCurdy, *J. Phys. B* **43** (2010).
[41] M. Liertzer, J. Feist, S. Nagele, and J. Burgdörfer, *Phys. Rev. Lett.* **109**, 013201 (2012).

- [42] L. Argenti, R. Pazourek, J. Feist, S. Nagele, M. Liertzer, E. Persson, J. Burgdörfer, and E. Lindroth, *Phys. Rev. A* **87**, 053405 (2013).
- [43] L. Yue and L. B. Madsen, *Phys. Rev. A* **88**, 063420 (2013).
- [44] C. M. Granados-Castro and J. L. Sanz-Vicario, *J. Phys. B* **46**, 055601 (2013).
- [45] L. Yue and L. B. Madsen, *Phys. Rev. A* **90**, 063408 (2014).
- [46] F. L. Yip, A. Palacios, F. Martín, T. N. Rescigno, and C. W. McCurdy, *Phys. Rev. A* **92**, 053404 (2015).
- [47] V. Majety and A. Scrinzi, *Photonics* **2**, 93 (2015).
- [48] A. Zielinski, V. P. Majety, and A. Scrinzi, *Phys. Rev. A* **93**, 023406 (2016).
- [49] F. M. Pont, A. Bande, and L. S. Cederbaum, *J. Phys. Cond. Matt.* **28**, 075301 (2016).
- [50] V. P. Majety and A. Scrinzi, *Phys. Rev. A* **96**, 053421 (2017).
- [51] S. Selstø and S. Kvaal, *J. Phys. B* **43**, 065004 (2010).
- [52] S. Kvaal, *Phys. Rev. A* **84**, 022512 (2011).
- [53] S. Selstø, T. Birkeland, S. Kvaal, R. Nepstad, and M. Førre, *J. Phys. B* **44**, 215003 (2011).
- [54] U. De Giovannini, D. Varsano, M. A. L. Marques, H. Appel, E. K. U. Gross, and A. Rubio, *Phys. Rev. A* **85**, 062515 (2012).
- [55] M. Feit, J. Fleck, and A. Steiger, *J. Comput. Phys.* **47**, 412 (1982).
- [56] G. Gumb, G. R. Ažin, and M. Pepper, *Phys. Rev. B* **60**, R13954 (1999).
- [57] S. Bednarek, B. Szafran, T. Chwiej, and J. Adamowski, *Phys. Rev. B* **68**, 045328 (2003).
- [58] O. Ciftja and M. G. Faruk, *J. Phys. Cond. Matter* **18**, 2623 (2006).
- [59] S. Selstø, *J. Phys. Cond. Matter* **25**, 315802 (2013).
- [60] G. C. Wick, *Phys. Rev.* **80**, 268 (1950).